A study of the electrical charging of the Rosetta orbiter: 2. Experimental tests in a laboratory plasma

Jean-Jacques Berthelier, Jean-François Roussel

A study of the electrical charging of the ROSETTA orbiter: 2. Experimental tests in a laboratory plasma

Jean-Jacques Berthelier
Centre d'étude des Environnements Terrestre et Planétaires, IPSL, CNRS-UVSQ, Saint-Maur, France

Jean-François Roussel
Office National d'Etudes et de Recherches Aérospatiales, Toulouse, France

Received 8 January 2003; revised 15 October 2003; accepted 30 October 2003; published 13 January 2004.

[1] Following the numerical simulation presented in the companion paper, we have performed experimental tests in a plasma simulation chamber to check the results of the numerical model and validate its capability to properly predict the electrical equilibrium of the Rosetta orbiter. Since low temperature cometary plasmas cannot be directly reproduced in such a chamber, we conducted the tests in plasmas with scaled characteristics deduced by considering similarity laws as is done in wind tunnel experiments. A mock-up of the Rosetta orbiter and solar panels was constructed with the capability of measuring collected currents over the various faces of the mock-up. These measurements included the possibility of observations on finer scales typical of ion collection as measured by ion energy analysers. This series of tests has allowed us to validate the performances and the predictions of the model presented in the companion paper. *INDEX TERMS:* 6099 Planetology: Comets and Small Bodies: General or miscellaneous; 7819 Space Plasma Physics: Experimental and mathematical techniques; 7894 Space Plasma Physics: Instruments and techniques; 7855 Space Plasma Physics: Spacecraft sheaths, wakes, charging; *KEYWORDS:* laboratory plasma simulation, plasma chamber experiments of S/C interaction with a cometary plasma

Citation: Berthelier, J.-J., and J.-F. Roussel (2004), A study of the electrical charging of the ROSETTA orbiter: 2. Experimental tests in a laboratory plasma, *J. Geophys. Res.*, *109*, A01105, doi:10.1029/2003JA009834.

1. Introduction

[2] During the last 20 years, a number of laboratory experiments have been realized to reproduce conditions encountered in space plasmas and compare laboratory measurements with in situ observations or with numerical models. Many of these experiments attempted to study the perturbations of the plasma surrounding LEO satellites which arise from their orbital motion and, possibly, to simulate and study charging effects [*Wright et al.*, 1985; *Coggiola*, 1998; *Vannaroni et al.*, 1992; *Svenes and Troim*, 1994]. Others aimed at reproducing space plasma processes such as double layers [*Baker et al.*, 1981] and beam-plasma interaction [*Kellog et al.*, 1982; *Bernstein et al.*, 1983; *Tsutui et al.*, 1984] or checking the operation of plasma probes [*Koons et al.*, 1984]. In the field of cometary physics, the KOSI experiment was set up a decade ago in a space simulation chamber to study the physics of cometary surfaces and the outgassing processes of the nucleus [*Grün et al.*, 1991; *Hesselbarth et al.*, 1991; *Kömle et al.*, 1991] but no attempts were made to generate a plasma from the neutral gas. In parallel with the numerical modeling reported in the companion paper [*Roussel and Berthelier*, 2003, hereinafter referred to as paper 1], we have undertaken an experiment in a plasma chamber to simulate the interaction between the orbiter and the cometary plasma flow. The main objective was to assess the validity of the numerical modeling by comparing laboratory data with results from the model run with the laboratory boundary conditions, i.e., plasma parameters and voltages on the mock-up. The idea was therefore to have laboratory conditions that allow one to simulate as closely as possible the conditions of the interaction of the positively charged ROSETTA orbiter with the cometary plasma. Position 1 of the orbiter, between the nucleus and the Sun (see paper 1), is of highest interest because it will be the position of the spacecraft during the major part of the operational phase. We therefore performed the laboratory experiments with a mock-up of the orbiter positioned accordingly. Furthermore, since the currents collected by the spacecraft from the cometary plasma, and thus its electrical equilibrium, are controlled by the structure of the plasma sheath looking towards the nucleus, we focused, in the laboratory, on the simulation and measurements of the plasma sheath on the side of the mock-up facing the plasma source in the chamber which is used to generate a simulated cometary plasma flow.

[3] Most of the laboratory plasma experiments related to space science which were cited above were devoted to producing conditions experienced by ionospheric satellites, thus quite different from those expected in the cometary coma. The first problem which we had to solve was to determine which plasma conditions can be realized in

0148-0227/04/2003JA009834

Table 1. Parameters on Ground and in Space and Scaling Factors

Parameters	Cometary Plasma	Scaling Factor	Laboratory Plasma
Ion mass	$M_i = 19$ (H_30^+)	m_i	$M'_i = 40$ (Ar^+)
Electron mass	M_e	$m_e = 1$	$M'_e = M_e$
Ion density	N_i ($\sim N_e$) $\sim 10^3$–10^5/cm^{-3}	n_i ($=n_e$) $= n$	N'_i ($\sim N'_e$) $\sim 10^4$–10^6/cm^{-3}
Electron density	$N_e \sim 10^3$–10^5/cm^{-3}	$n_e = n$	$N'_e \sim 10^4$–10^6/cm^{-3}
Ion temperature	$T_i \sim$ 50K	t_i	$T'_i \sim$ 800 K
Electron temperature	$T_e \sim$ 50K	t_e	$T'_e \sim$ 1500–3000 K
Ion drift velocity	$V_i \sim$1 km/s	v_i	$V'_i \sim$ 5 km/s
Electric potentials	$\Phi \sim$ 1.5–4 volts	φ	Φ' (see Table 3)
Characteristic dimension	L $\sim$ 2m	l	L$'$ $\sim$ 0.3m
Magnetic field	B = 0	N/A	B$'$ < 2 μT (within 1 m of diameter)

practice that are adequate to simulate the physics of the interaction between the orbiter and the cometary plasma and are able to allow a meaningful comparison with the numerical model. This problem is discussed in section 2. Section 3 is devoted to a short description of the mock-up of the orbiter and the simple instrumentation which was used for this initial round of measurements. Finally, in section 4, we report the main experimental results and compare them to those obtained from the numerical model.

2. Experimental Simulation of a Cometary Plasma: Scaling Laws and Practical Limitations

[4] Conditions typical of the ionosphere, in an altitude range from 400 km to 1500 km, are quite easily reproducible in simulation chambers. The JONAS chamber is located at ONERA/CERT in Toulouse and consists of a cylindrical tank 1.8 m in diameter and 3 m in length. A high performance pumping system maintains the pressure near 10^{-6} Torr when the source is operated. The plasma source is a Kaufman ionization source operated with argon, since this gas is chemically inactive and can be ionized under the form of singly charged ions with a good efficiency due to its rather low ionization potential. Ions exiting the source are accelerated to energies of about 5 to 20 electron volts and this ion beam is neutralized by electrons emitted from a heated filament. The resulting plasma expands in the chamber where relatively homogeneous conditions are obtained in the vicinity of the center of the chamber, within a volume of approximately 1.2 m in diameter and 2 m in length. The typical plasma densities and thermal electron temperatures range from about 10^4 to 10^6 el/cm^3 and from 1000 K to 6000 K, respectively, while the ion drift velocity varies typically from $\sim$3 to $\sim$8 km/s. A summary of the main plasma characteristics and diagnostics in JONAS have been published by *Roussel et al.* [1997]. The plasma conditions which are expected in the inner coma of comet Wirtanen have been reviewed in paper 1. For an active comet, the expected cometary densities in the range of distances from the nucleus that will be spanned by the Rosetta orbiter lie in the range of $\sim 10^3$ to 10^5 el/cm^3 thus not far from plasma densities typically obtained in JONAS. Plasma flow velocities in the inner coma range from a few hundreds meters/s to 1 km/s at most, significantly less than the values quoted above. However the parameter which displays the largest difference between cometary conditions and those in the plasma chamber are the temperatures since the temperature of thermal cometary electrons and ions is expected to be about 50 K in the range of distances from the nucleus of interest for the mission [*Mendis et al.*, 1985]. It is therefore not possible to reproduce in a plasma chamber such as JONAS conditions identical to those expected during the Rosetta mission. Simulating cometary conditions therefore leads to a situation that is generally encountered in experimental studies of gas dynamics in aerodynamic wind tunnels. It is necessary (1) to determine by means of similarity laws how the cometary conditions can be scaled in the laboratory and (2) to find the combination of laboratory parameters that can be achieved in practice in order to allow meaningful experiments to be performed. To our knowledge, this question has not been formally investigated in laboratory experiments such as those cited above. It has been examined by *Podgornyi and Sagdeev* [1970] and *Erukhimov and Genkin* [1992] in a reverse situation where the authors looked at using the ionosphere as a laboratory for plasma physics investigations.

2.1. Scaling Laws

[5] Let us define the cometary parameters by capital letters, the laboratory parameters by capital letters with a prime, and the scaling parameters (which are the ratio of laboratory to cometary parameters) by lower-case letters. The definition of all scaling parameters is given in Table 1. As an example, the scaling parameter n_e for the electron density is $n_e = N'_e/N_e$. As a further example, in the inner coma H_30^+ ions are the major species while tests in the JONAS chamber will be conducted using argon: this gives a value of 2.1 for the m_i parameter. The other scaling parameters are also indicated in Table 1 for information, but the relations and numbers of interest, which relate to the scaling process and to the similarity laws, are those indicated in Table 2.

[6] The determination of the relations between the scaling parameters can be addressed through either a physical approach which addresses physical dimensionless numbers conservation (Mach number, etc.), or a mathematical approach which takes into account the dimensional equations derived from the Vlasov and Poisson equations that govern the system. Both approaches are described in detail below. In practice both of them result in the same set of ratios r_i given in Table 2. Theoretical values of these ratios are 1 (except r_4) and we have indicated in the last column the values that have been actually achieved during the laboratory tests.

[7] The physical approach follows from the constraints that should be imposed on the laboratory parameters in order to properly take into account the physics of the problem and the relative magnitude of the parameters that

Table 2. Dimensionless Numbers to be Conserved (Constraints 1 to 3) and ***B*** Field Inequality Constraint (4)

Constraints Imposed to Laboratory Plasma Parameters	Relations Between Scaling Factors	Typical Values in the Laboratory
1- Ion Mach number unchanged	$r_1 = m_i v_i^2/t_i = 1$	$r_1 \sim 1.5$
2- Kinetic and potential energies:		
2.1- Ions (bulk energy)	$r_{2,1} = \varphi/m_i v_i^2 = 1$	$r_{2,1} \sim 0.3$
2.2- Electrons (thermal energy)	$r_{2,2} = \varphi/t_e = 1$	$r_{2,2} \sim 0.2$
3- Ratio of Debye length and characteristic dimension unchanged	$r_3 = l^2 n/t_e = 1$	$r_3 \sim 1$
4- Magnetic field negligible (electron gyroradius $\gg$ characteristic dimension)	$r_4 = (2m_e k T_e)^{1/2}/eBL \gg 1$	$r_4 \sim 2$

control the interaction of the orbiter with the surrounding plasma. The first and most important parameter which appears in Table 2 is the Mach number which describes the plasma flow. Requiring the cometary value to equal the laboratory value leads to the ratio r_1 as shown. Also, the kinetic and potential energies must scale similarly. For the ions, the bulk energy is much larger than the thermal energy and is therefore the energy to be considered, hence the ratio $r_{2,1}$. For the electrons, on the other hand, the bulk velocity is negligible compared to the thermal velocity, leading to $r_{2,2}$. The parameter r_3 requires that the ratio of Debye length to orbiter characteristic dimensions remains the same, while the condition on r_4 allows us to neglect any magnetic field effects.

[8] All together, the previous set of four relations can be summarized by the four equations:

$$\varphi = t_e = t_i = m\, v_i^2 = n\, l^2 \tag{1}$$

which leaves 2 degrees of freedom for the total set of six scaling parameters n ($= n_i = n_e$), t_e, t_i, v_i, φ, and l. These two free scaling parameters gave us enough flexibility to define the experimental conditions within the reachable range of standard values for routine operation of the source.

[9] The condition on the magnetic field is rather simple: there is no magnetic field in the inner coma inside the contact surface and laboratory simulations must be made in an unmagnetized plasma or at least under conditions where the magnetic forces are negligible compared with electric forces. This is in fact equivalent to having particle gyroradii much larger than the characteristic dimension of the mock-up. This condition is more restrictive for electrons for which it can be written as inequality 4. In practice, the magnetic field in the JONAS chamber is controlled using a set of three orthogonal Helmholtz coils that compensate the terrestrial magnetic field over a fairly large volume encompassing the region of interest for the experiment. Measurements, displayed in Figure 1, show that the intensity of the residual magnetic field is reduced to less than about 20 mG (2 μT) in a region ~1 m in diameter and of extent ~1 m along the axis. At distances up to 1 m from the axis the magnetic field intensity is less than ~50 mG. Equality 4 is thus roughly satisfied.

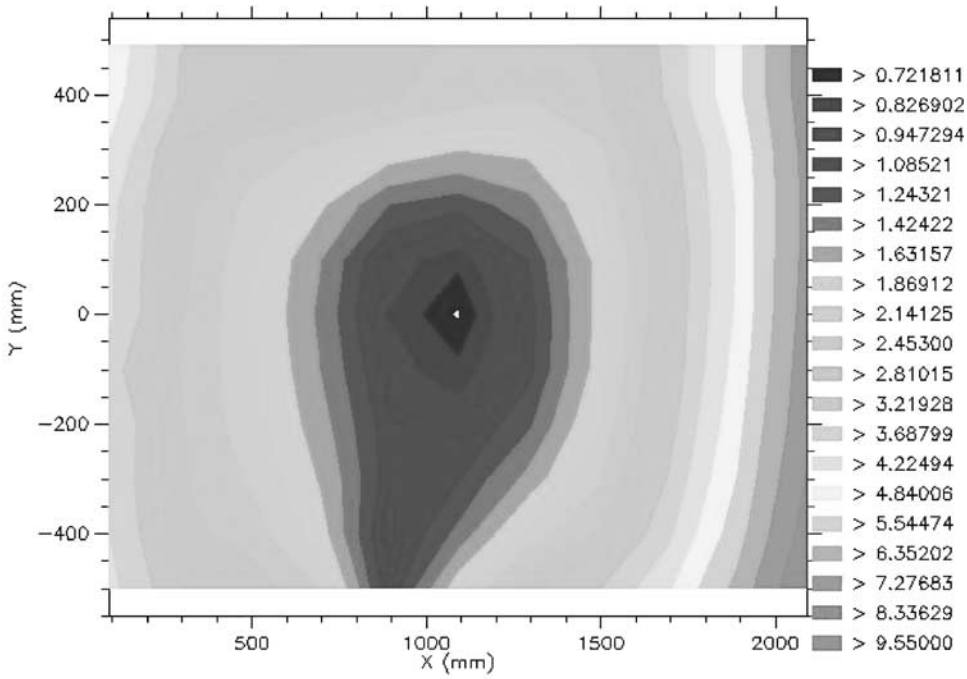

Figure 1. Norm of the compensated magnetic field in the symmetry plane of JONAS chamber (μT). See color version of this figure at back of this issue.

[10] Scaling laws can also be determined by a mathematical approach using the Poisson and the steady state ($\partial/\partial t \equiv 0$) Vlasov equations which govern the dynamics of the plasma in the collisionless limit applicable to the experiment. This mathematical approach provides a check of the physical approach. The Poisson equation is

$$\nabla^2\Phi = -e(Ni - Ne)/\varepsilon_0 \tag{2}$$

and the steady-state Vlasov equation for charge species α is

$$\mathbf{v}.\vec{\nabla}\mathbf{f}_\alpha + \frac{q_\alpha}{M_\alpha}(\mathbf{E} + \mathbf{v}\times\mathbf{B})\cdot\vec{\nabla}_v\mathbf{f}_\alpha = 0, \tag{3}$$

where α stands for ions or electrons. To obtain the relations linking the scaling factors, we are interested in the dimensional equations that can be derived from equations (2) and (3). We can thus simplify the Vlasov equation for charge species α and express it in a one-dimensional approximation:

$$v.\frac{\partial f}{\partial L} + \frac{q_\alpha}{M_\alpha}\left(-\frac{d\Phi}{dL} + \mathbf{v}x\mathbf{B}\right)\frac{\partial f_\alpha}{\partial v} = 0 \tag{4}$$

and use the classical dimensional formulation to replace $\partial/\partial L$ by $1/L$ and $\partial/\partial v$ by $1/\mathbf{v}$ so that the dimensional equations can finally be written as:

$$\Phi/L^2 = -e(N_i - N_e)/\varepsilon_0 \tag{5}$$

$$vf_\alpha/L - \frac{q_\alpha}{M_\alpha}(\Phi/L)f_\alpha/v + \frac{q_\alpha}{M_\alpha}(vB)f_\alpha/v = 0. \tag{6}$$

Equations (5) and (6) must be kept unchanged by the scaling process. Equation (5) yields:

$$\varphi/l^2 = n. \tag{7}$$

Taking into account that B $\sim$ 0, the comparison of the first two terms of equation (6) yields

$$v/l = \varphi/(m_\alpha l v), \tag{8}$$

which can be expressed for both the ion drift velocity and the ion and electron thermal velocities, hence the relations:

$$\varphi = mv_i^2 = t_e = t_i. \tag{9}$$

Clearly, the combination of equations (7) and (9) provides a set of equations identical to those expressed in equation (1). Finally, the last two terms of the Vlasov equation (6) give the constraints on the magnetic field already expressed by relation 4 in Table 2.

2.2. Practical Limitations

[11] The major limitation comes from the impossibility of applying the same scaling laws adopted for the plasma ions and electrons to photoelectrons. This arises because the characteristic energy of photoelectrons does not change when going from the space environment to the laboratory and therefore is not consistent with the scaling choices applied to the other species. We have thus conducted the tests in the chamber and the accompanying numerical simulations without photoemission. As expected, and demonstrated in paper 1, the basic effect of the photoelectron emission is to drive the spacecraft potential to positive values. When the spacecraft is in position 1 (between Sun and comet, see companion paper) and with average Debye lengths, trajectory calculations have shown very few photoelectrons emitted from the sunward side of the spacecraft and solar panels bend towards the opposite side: the photoelectrons have therefore no significant influence on the structure of the plasma sheath on the side of the spacecraft looking towards the nucleus. As mentioned in the introduction, the laboratory experiments were performed to validate the model computation concerning this part of the sheath. Therefore introducing an actual photoemission is not necessary since the photoelectrons have no significant effect on the sheath structure. Of course, the floating potential that results from the photoemission has to be taken into account by applying positive potentials on the mock-up. Several sets of potentials were applied to the mock-up faces (see section 3) to simulate various levels of charging of the orbiter and check the numerical model over a large domain of conditions.

[12] Other limitations arise from the limited range of plasma parameters that can be achieved in practice in the JONAS chamber. In the laboratory the standard ion Mach numbers are in the range from 7 to 12 due to the difficulty in achieving a stable operation of the ion source at an acceleration voltage less than about 5 volts. The tests reported in this paper were done with a value of $\sim$7.5, higher than the typical value of 4.5 which was adopted in paper 1. Another difference comes from the anisotropy of the laboratory ion thermal distribution with a temperature parallel to the flow of $\sim$800 to 1000 K, higher than the temperature in the perpendicular direction which is about $\sim$400 to 600 K, as deduced from the ion angular distribution measured in the undisturbed plasma. The ratio of the electron and ion parallel temperature ranges from 2 to 4 in the chamber, rather higher than the cometary values which are expected to vary from 1 to 2. As far as the ratio between the typical length of the system and the Debye length is concerned, satisfactory solutions were achieved. With 2 m as the typical dimension of the orbiter and width of solar arrays and a Debye length in the range from 0.2 to 20 cm, this ratio varies from 10 to 1000 in the coma. Corresponding numbers in the laboratory are 30 cm and 0.1 to 5 cm, respectively, with a ratio in the range from $\sim$6 to 300 thus within the range of cometary conditions. For most of the laboratory tests, the Debye length was about 0.9 cm and the ratio between the characteristic dimension and the Debye length equal to 33. As indicated above, thermal electron gyroradii of $\sim$2 m in the chamber obtained by reducing the magnetic field are significantly larger than the characteristic dimension of the mock-up of 30 cm. Very large positive potentials cannot be imposed on the mock-up because the sheath grows and interacts with the walls of the chamber and, more importantly, because the electron currents that are collected by the mock-up increase to a point where the plasma source itself cannot work properly (see section 4). Even if the laboratory experiments were more representative of the case of moderate charging of the Rosetta orbiter compared with the highest charging conditions deduced from the numerical model, the laboratory floating potentials are still very large (about 30 to 50 times) compared with the ion and electron thermal energies which is a basic feature of the expected cometary conditions. As it was reported in

Table 2, the actual plasma parameters in the laboratory yet yielded correct values for the numbers to be conserved (coefficients r_1 to r_3 close to 1, and r_4 larger than 1).

[13] To summarize, even if a perfectly scaled simulation of the cometary conditions is not fully achievable in the JONAS chamber, it is nevertheless possible to reach plasma conditions that are representative of the physics of the problem, in particular the high Mach number of the ion flow, the ratio between the characteristic dimension of the system and the Debye length, and the positive charging of the orbiter at values that are large compared with the ion and electron thermal energies. This allowed us to compare experimental and model results for conditions which are physically sound and to perform a valuable check of the validity of the numerical model. During the experimental tests, the plasma parameters were measured in the undisturbed plasma flow ahead of the sheath surrounding the mock-up. They were used to define the characteristics of the electron and ion populations which are injected in the simulation box making the numerical model perfectly representative of the actual boundary conditions of the laboratory experiments. For the sake of completion, a last point may be mentioned which relates to the "cold" ion population in the chamber. These ions are created by charge exchange between the drifting ions and the cold neutral gas. They have been observed in JONAS by *Roussel et al.* [1997] and their current density, rather small and only about 5% of the current density of the drifting ions, has only a noticeable effect in the wake of an object from which drifting ions are excluded. We did not take them into consideration in the simulation since an accuracy of a few percent is beyond the goal of the present study.

3. Description of the Experiment

[14] A schematic illustration of the experimental set-up in the JONAS plasma chamber is shown in Figure 2. Two series of tests have been performed. In the first one, a two-dimensional (2-D) case was simulated with a mock-up of the solar panels 1 m long and 20 cm wide. The two sides of this plate were electrically insulated in order to allow the simulation of a 2-D "insulator" electrical configuration as referred to in paper 1. The purpose of this preliminary experiment was mainly to check, by means of simple Langmuir probe measurements in the vicinity of the mock-up what perturbations arise from various amplitudes and configurations of polarizations applied on the two sides of the plate. A few comparisons have also been performed with the results of a 2-D numerical simulation.

[15] The second series of tests were conducted with a 3-D mock-up of the orbiter consisting of a cube with a side length of 20 cm simulating the orbiter body and two plates 20 cm wide and 50 cm long representing the solar panels. The results of the numerical simulation displayed in paper 1 have shown that the sheath around the orbiter body and the sheath around the solar panels are fairly well decoupled at distances larger than about 20 Debye lengths. Similarly, the disturbances of the sheath of the solar panels due to the end effect at their far edge vanish at a similar distance. All together, the geometry of the mock-up seems therefore appropriate and should not induce uncontrolled effects on the experimental simulation as long as the Debye lengths in the chamber stay smaller than 1 cm which was the case during the tests. The two sides of the plate simulating the solar panels are electrically insulated and can be biased separately. Similarly, the face of the cube opposite to the plasma source, which corresponds to the face of the orbiter looking towards the Sun, is electrically insulated from the other five faces. Such a design aims at simulating the "insulator" electrical configuration referred to in paper 1 and which was shown to provide a way to reduce the positive equilibrium potential of the orbiter body which is detrimental to charged particle measurements. The mock-up was placed near the center of the chamber in the region where the terrestrial magnetic field can be compensated and reduced to small enough values (see section 2). Currents collected by all mutually electrically insulated surfaces of the solar panels or orbiter body can be measured independently. During the tests several different sets of potentials (see Table 3) were applied to the mock-up in order to check the accuracy of the model over a large domain of conditions. In particular, in addition to the positive potentials that are of primary interest to reproduce the positive charging of the orbiter, we have also used negative biasing potentials since they allow a thorough validation of the numerical model under quite different conditions.

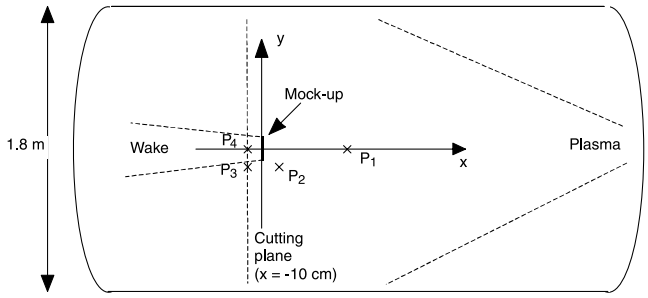

Figure 2. Schematic view of the JONAS chamber, two-dimensional (2-D) or 3-D Rosetta mock-up, and location of Langmuir probe measurements.

[16] The face of the cube facing the plasma source has a circular hole in its center through which particles gain access to the entrance area of a plasma spectrometer located inside the cube and designed to measure the angular and energy distribution of the incoming ions. This spectrometer consists of three parts: (1) the entrance section made of a tandem of two parallel plate analyzers following each other which allows varying the direction of sight of the instrument over a total field of view of about a 30° half angle, (2) a cylindrical analyzer which particles enter after exiting the entrance section. It selects the energy of the analyzed particles, (3) a detector using an MCP to measure the current due to the particle fluxes. The instantaneous field of view of the spectrometer is ~3° half angle for all directions, the two angles defining the line of sight can be varied by steps of ~1.5° and the energy resolution is ~15%.

4. Experimental Results

4.1. Two-Dimensional Measurements

[17] It is well known that in simulation chambers like JONAS, abnormal plasma conditions arise if too much electron current is drawn from the plasma by collectors

Table 3. Current Collected by the Four Mock-Up Conductors (Body/Solar Panels, Sun/Comet Face) for Seven Bias Configurations and Comparison Between Experiment and Simulations

Imposed Potentials, V		Collected Currents, μA							
		Solar Array				Main Body			
		Comet Side		Sun Side		Comet Side		Sun Side	
Comet Side	Sun Side	Simulation	Experiment	Simulation	Experiment	Simulation	Experiment	Simulation	Experiment
−5	−5	13	13	0.02	0.90	12	14	0.01	0.40
−2	−2	13	12	0.00	0.40	9	10	0.00	0.00
2	2	−857	−810	−381	−240	−1632	−1240	−79	−37
6	6	−1522	−1530	−581	−610	−1895	−2170	−116	−94
−5	15	16	16	−1942	−1570	15	17	−602	−400
−2	15	16	15	−1951	−1570	13	13	−641	−400
2	15	−745	−590	−1633	−1680	−752	−900	−504	−630

placed in the chamber. The first noticeable effect is detected on the electron temperature which increases when the plasma in the chamber is deprived of electrons. When the collected electron current gets above some threshold, the plasma is definitely non-Maxwellian and eventually a limit is reached when the source operation is not possible any more. That threshold is related to the ratio between the collected current and the thermal current that can be brought by an unperturbed Maxwellian plasma. The former must be "negligible" compared to the latter. A plasma of density of 5×10^5 el/cm^3, as the one considered here, can conduct about 25 mA/m^2, hence about 60 mA through a whole section of the chamber. From a practical point of view, the plasma source working parameters and the aspect of Langmuir probe characteristics in the 2-D experiments led us to determine a threshold value of 15 mA that the collected electron current must not exceed in order that proper operation of the chamber is maintained. This is completely consistent with the previous theoretical argument, stating that the collected current was to be "negligible" compared to 60 mA. By comparison the total electron current collected by the mock-up in the 3-D tests is 4 mA when charged to +6 Volts, still well below that reasonable threshold.

[18] Conventional Langmuir probe measurements have been performed at a number of locations both in front and in the wake of the plate. A typical current/voltage characteristic is shown in Figure 3. It was obtained in the case of a plasma with an electron density of 5.5×10^5 el/cm^3 and an electron temperature of ~3000 K, corresponding to a Debye length of 5 mm, and an ion drift energy of 5.5 eV equivalent to a drift velocity of 5 km/s. From such curves, values of the plasma parameters as well as the local plasma potential, corresponding to the peak in the current first derivative, can be deduced. For this example, the probe was located 50 cm ahead of the mock-up polarized at +20 Volts. The Langmuir characteristic is globally similar to a classical trace, with yet distinct differences in the shape of the derivative above the plasma potential: the derivative is increasing above 3 Volts, whereas probe models usually predict decreasing dI/dV derivatives. It indicates that the measurements are taken in the presheath region in the presence of a disturbed electron distribution function.

[19] The estimated value of the local plasma potential is ~1.7 Volts (inflection point). Measurements conducted at the same location with a grounded mock-up give a value of 0.3 Volts for the potential, in that case practically equal to the plasma potential measured in the case of a chamber with an undisturbed flowing plasma and no obstacle. The small increase of potential (+1.4 V) due to the polarization of the mock-up was expected due to the presheath characteristics, a small positive potential in an almost unperturbed plasma which attracts electrons from a distance to the sheath itself. Another possible contribution to that small potential increase is the functioning of the emitting filament. When little current is extracted from it, only its most negative extremity is emitting electrons, and the other ones are reattracted by the filament. When more electrons need to be extracted, the plasma potential around it goes up to extract electrons from a longer part of the filament. That certainly contributes to the observed increase of potential but also to the heating of the plasma electrons, since they are emitted from the whole length of the filament between its most negative end, at 0V and nearly its other end at ~+1.7 Volts.

[20] A series of measurements were made across the wake region, in the cutting plane indicated in Figure 2. We used classical interpretation methods. For ions, the ion branch is linearly interpolated to the plasma potential. At plasma potential the plasma is not disturbed by the probe and this current is given by the product of plasma density, ion velocity, and probe cross section, which allows one to

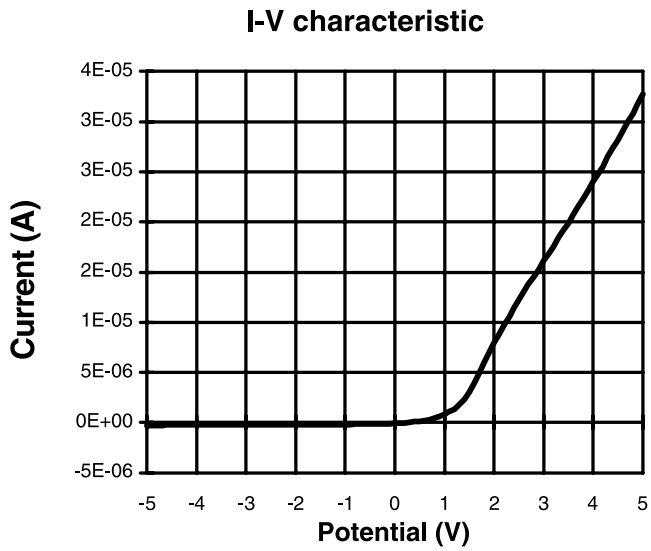

Figure 3. Current/Voltage characteristic of a Langmuir probe at 50 cm upstream of the 2-D mock-up.

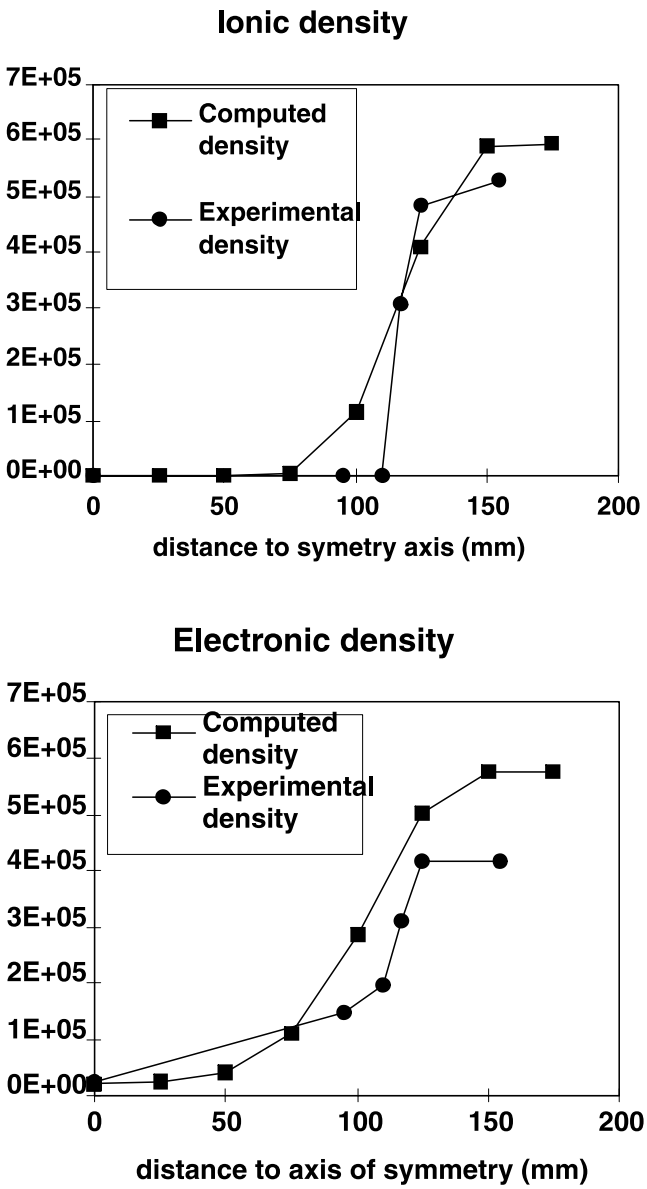

Figure 4. Ion and electron density profiles on the cutting plane of Figure 2, comparison between simulation and experiment.

obtain the ion density. Similarly, for electrons density is inferred from current at plasma potential, where plasma is undisturbed. However, due to the very large plasma perturbation in this region, these methods based on the assumption of the probe embedding in an unperturbed plasma are certainly subject to significant errors.

[21] Nevertheless results on the ion and electron densities have been displayed in Figure 4 and compared to values obtained from the 2-D model. In spite of the limited accuracy of the experimental data, there is a fairly good agreement between the two sets of data indicating that the 2-D simulation is certainly close to reality even in the most disturbed part of the sheath.

4.2. Three-Dimensional Measurements

[22] In this series of measurements, the undisturbed plasma parameters were the following: electron density 1.4×10^5 el/cm^3, electron temperature $\sim$4000 K, ion drift energy $E_{c_{\text{ions}}} = 5.5$ eV $\pm$ 1 eV, ion temperature parallel to the flow $T_{\|} \sim 800$ K, perpendicular to the flow $T_{\perp} \sim 300$ K as deduced from the ion flow divergence of $\sim 3°$. These values were used to define the characteristics of the injected particles in the numerical simulations to which the measurements were compared.

4.2.1. Global Current Measurements

[23] The simplest experimental data are the currents collected by each of the four independently polarized areas of the external surfaces of the mock-up. They provide a comparison on a global scale between the experiment and the numerical model. Several different potential configurations were imposed on these four elements in order to vary both the electrical configuration and the level of applied voltages. They are indicated in Table 3 which provides an overview of the results. The first four cases correspond to the nominal electrical configuration of the equipotential Rosetta spacecraft with all external surfaces at the same potential. Applied potentials vary from large (-5 V) negative potentials to large (+6 V) positive potentials. The last three cases correspond to the ''insulator'' configuration with different potentials applied to the surfaces looking towards the plasma source (i.e., toward comet nucleus) referred to as the ''front faces'' and in the opposite direction (i.e., toward the Sun) referred to as the ''rear faces.'' These three cases have in common the same potential of +15 V applied to the rear faces, while the potential of the front faces vary from -5 V to +2 V. Graphical illustrations are given for three cases in Figures 5, 6, and 7 in order to allow a clearer overview of the main results. All these measurements were made with similar plasma conditions in the chamber with nevertheless random temporal variations of about $\pm$10% for the unperturbed plasma density due to the nonperfect stability of the plasma source. The first general conclusion which can be drawn is that there is a very satisfactory agreement between the experimental and the modeled currents, probably on the order of $\pm$15% if one takes into account the fluctuations of the plasma during the measurements. One must note, in particular, that the agreement is equivalently good for a negatively or a positively biased mock-up which demonstrates that the numerical simulation correctly models the ion as well as the electron dynamics which is important to guarantee the validity of the floating potential calculation. The larger discrepancy between measured and modeled current on the rear face (sunward looking side) of the orbiter body comes at least in part from the presence of a boom, attached to this face and used to hold the whole mock-up, which disturbs particle collection. As can be seen by comparing the first three cases and the last three cases, large variations of the potential applied to the rear faces, from -5 V to +15 V have only a slight effect on the current collected by the front faces, indicating that the global extent and structure of the sheath surrounding the front faces are not significantly affected by the potential of the rear faces, as expected from the results shown in paper 1. Both the experiment and the numerical simulation demonstrate that the two sides of the orbiter and solar panels behave rather independently, a result which confirms the idea put forward in paper 1 showing the interest of electrically separating the front and the rear faces. The small increase observed in the ion current collected by the front

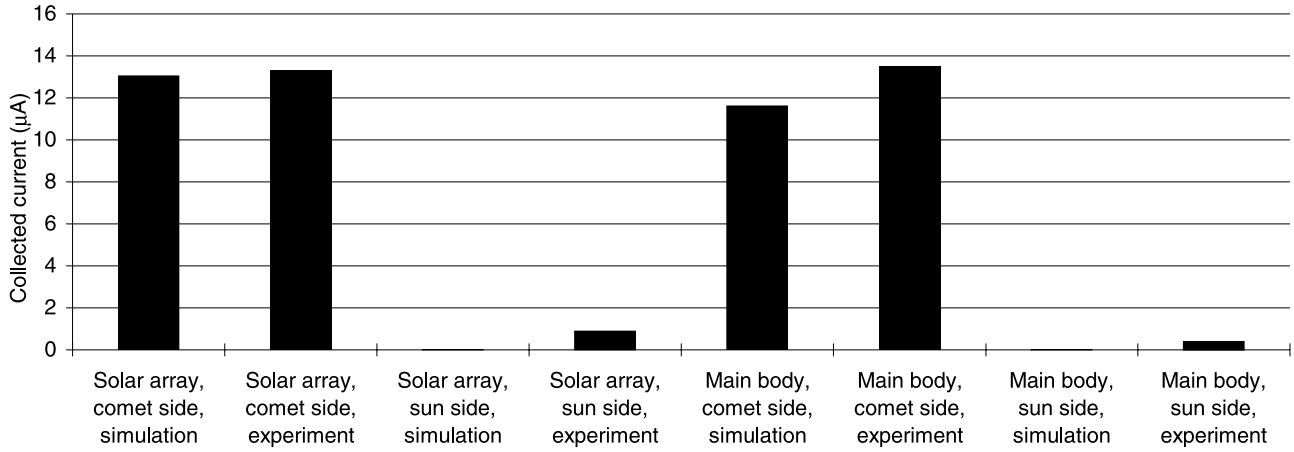

Figure 5. Measured and computed collected currents for an equipotential mock-up at −5 Volts.

face for higher potential on the rear face can be explained by a focusing effect on the ion trajectories due to the positive potential leaking towards the front face. This small effect is well reproduced in the numerical modeling. It is worth mentioning a last observation: no ions are collected by the rear face in the numerical simulation, since it is facing the wake. In the experiment, a small current is collected on the wake side, for example 0.4 μA on the rear face of the solar panel, as compared to ∼13 μA on the ram side. As already mentioned, this wake current can be explained by the collection of the cold ions with a rather isotropic angular distribution which are present in the chamber but have not been introduced in the numerical simulation.

[24] An interesting feature can be noticed in Figure 6 drawn for the case of an equipotential mock-up with a positive potential of +6 V. The currents collected by the front face (oriented towards the ram) and the rear face (oriented towards the wake) of the solar panels are different by a factor of 2.5 approximately and the experiment and numerical simulation agree perfectly well. This is due to the absence of flowing ions in the wake which causes the electron attracted by the positive potential to build a negative space charge. This space charge prevents further access of thermal electrons to the wake thus reducing the electron collection by the rear face of the solar panels. This effect was already observed in results reported in paper 1 and explains the differences observed between position 1 and position 3 in the "insulator" electrical configuration. It is of interest to have been able to check this effect experimentally.

4.2.2. Ion Analyzer Measurements

[25] One of the objectives of the experimental tests in the JONAS chamber was to operate under conditions as close as possible to those encountered in the coma when the orbiter floats at a positive potential larger than both the thermal and drift energies of the ions. Under such conditions, no ion can reach an instrument with its entrance area at the positive (with respect to plasma) ground potential of the orbiter and measurements are meaningless. In an attempt to overcome this problem, an often-used countermeasure consists in polarizing the entrance area of particle detectors to a large enough negative voltage with the idea to overcome the repulsive effect of the positive spacecraft. This is, for example, what will be done for the ion spectrometers of the Rosina experiment on Rosetta. However, it is well known that for large enough spacecraft floating potentials and due to the big difference in size between the spacecraft and the entrance area of an instrument, potential barriers can develop in front of the instrument entrance. These potential barriers entail large and often unexpected deflection of the

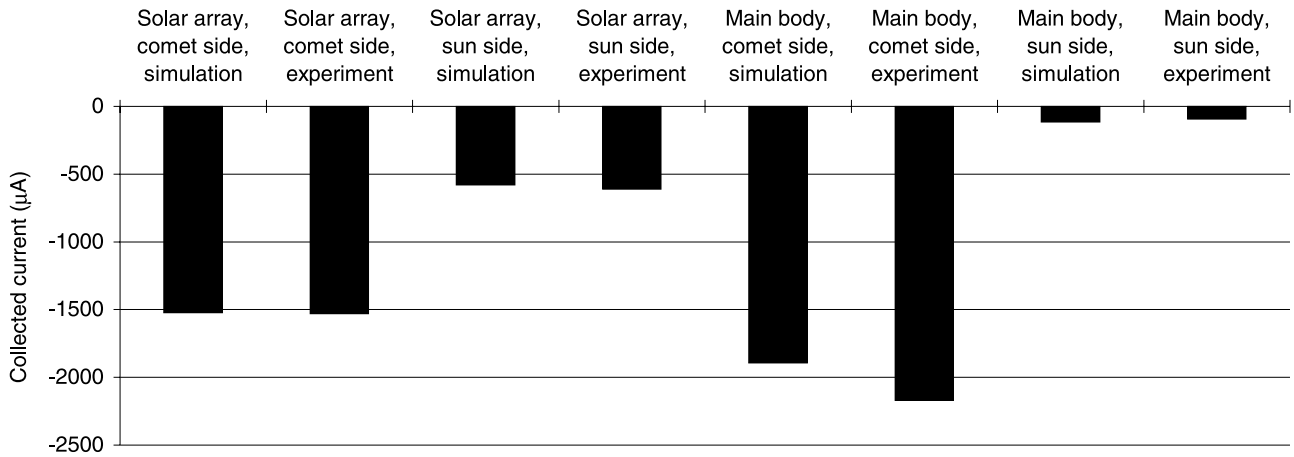

Figure 6. Measured and computed collected currents for an equipotential mock-up at +6 Volts.

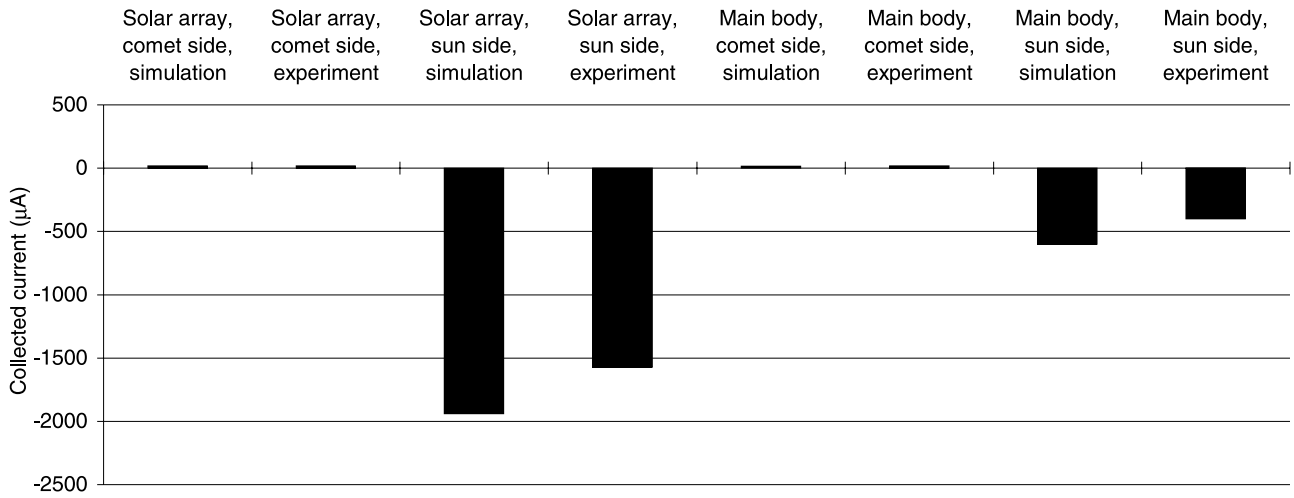

Figure 7. Measured and computed collected currents for a Sun side of the mock-up at +15 V and a comet side at −5 V.

ion trajectories [e.g., *Bourham et al.*, 2002; *Hamelin et al.*, 2002] and even may prevent particles with too low an energy from entering the instruments. During this first series of tests and using a simple geometry shown in Figure 8, we have tried to simulate the operation of an ion spectrometer with a polarized entrance surface sitting on a positively floating mock-up. As above, the idea was to check the capability of the numerical model to describe this situation and determine if it can provide accurate information in the actual conditions that will be met by Rosetta. In the experimental setup shown in Figure 8, the diameter D of the hole in the face of the orbiter mock-up looking towards the plasma source (i.e., towards the "comet nucleus") can be either 20 or 40 mm. The entrance area of the ion spectrometer is located just behind this hole at a distance of ~3.5 mm and its diameter is about 60 mm, so that this polarized area is always greater than the hole diameter.

4.2.3. Total Current Measurement at the Entrance of the Spectrometer

[26] These first measurements allow one to determine the total ion current impinging on the entrance surface of the spectrometer irrespective of the ion energy and direction of arrival. Several measurements were made varying the potentials applied to the orbiter mock-up and to the entrance of the spectrometer and results are presented in a graphical form in Figures 9 (D = 20 mm) and 10 (D = 40 mm) for both the experimental currents and the computed currents. All current intensities were normalized with respect to the current collected when both the mock-up and the entrance aperture of the spectrometer are at the ground potential of the plasma chamber, practically within less than 1 volt from plasma potential. Results have been represented in logarithmic units since the currents vary over two decades as a function of the potentials.

[27] With +6 V on the mock-up and 0 V on the spectrometer, the (6, 0) case, the collected current is larger than in the reference case where both the mock-up and the entrance area are at the chamber floating potential, the (0, 0) case. The negatively biased entrance area builds a potential structure in the nearby plasma sheath which focuses and attracts quite efficiently the incoming ions resulting in a larger collected current. However, this effect only exists as far as the potential on the mock-up does not exceed a threshold which is a function of the ion drift energy. When the potential applied to the mock-up increases

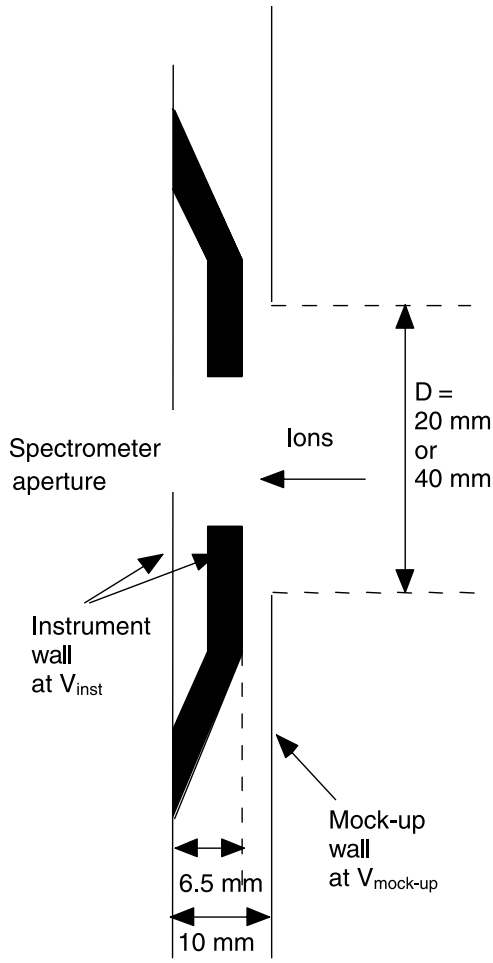

Figure 8. Detail of the spectrometer entrance.

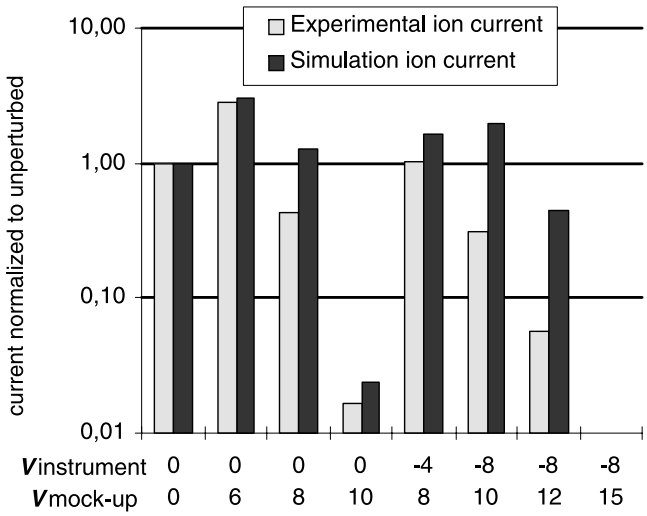

Figure 9. Comparison of measured and computed ion currents collected on the entrance area of the spectrometer. The various potentials applied to the mock-up ($V_{\text{mock-up}}$, lower line) and to the entrance area relative to the mock-up (V_{inst}, upper line) are indicated below the horizontal axis. Hole diameter in the face of the mock-up: 20 mm.

(+8 V and +10 V), the ion current decreases, for instance down to ~2% of the (0, 0) reference current in the case (10, 0). This indicates that a potential barrier builds up at some distance in front of the spectrometer aperture preventing practically all ions from reaching the spectrometer. As anticipated, when the spectrometer aperture bias goes more negative with respect to the mock-up, the current collection is enhanced: for example, with $V_{\text{mock-up}} = +10$ V, the current increases from 2% to 31% of the reference current when the spectrometer entrance bias goes from 0 V to −8 V, in fair agreement with the numerical simulation. This indicates that the potential barrier lies close to the entrance and is quite sensitive to the potential of the entrance area of the spectrometer. The comparison between numerical and experimental currents shows that the current collection is numerically overestimated by a factor of ~2 in the cases where there is a large difference between the potential on the mock-up and the potential on the entrance of the spectrometer. This can be understood by considering the difference between the actual experimental geometry, where the spectrometer aperture plane lies 3.5 mm behind the mock-up face, and the numerical geometry used in the simulation, where the spectrometer aperture lies directly in the plane of the mock-up face. This simplification was made because the finest possible mesh size of the numerical grid was 5 mm, due to CPU time and computer memory limitation, and the 3.5 mm distance was too small to be taken into account. In the laboratory experiment the actual voltage in the plane of the mock-up face is thus less negative than the spectrometer entrance bias, hence the reduced ion current collection. Also, the negative equipotential surfaces which extend in front of the hole are less developed.

[28] When the hole diameter is increased to 40 mm, the behavior of the currents and the agreement between simulation and experiment are rather similar. As can be expected the current enhancement due to the negative bias applied to the entrance is larger.

4.2.4. Ion Angular Distribution Measurements

[29] The ion spectrometer was also used to determine the angular distribution function of the impinging ions. An example of the data and of the numerical results is presented in Figure 11 for $V_{\text{mock-up}} = +8$ V and $V_{\text{instr}} = -4$ V. The selected ion energy was equal to the energy of flowing ions accelerated by the potential on the aperture of the spectrometer. The data from the spectrometer are output current measured on the detector as a function of the direction of sight of the instrument defined by the two angles in the vertical and horizontal planes. The faint X shape of the resulting angular distribution is due to the transfer function of the spectrometer which displays an enhanced sensitivity for directions of arrivals at 45° with respect to the main axis of the spectrometer. The main difference lies in the width of the angular distribution, about 3 to 4° half angle from the experimental data and 5 to 6° for the numerical results. Two reasons can explain at least in part this difference. As mentioned above, the actual position of the entrance plane in the experiment is behind the face of the mock-up, contrary to the simplified geometry used in the numerical model. The actual geometry entails a more efficient converging lens effect which focuses the incoming ions and reduces their angle of incidence. The second reason is linked to the 5 mm resolution of the numerical grid, too large to properly reproduce the exact potential variation in regions with small scale structures as is the case in the vicinity of the entrance area, or in the potential barrier area, in particular with consequences on the accuracy of the ion deflection modeling.

5. Conclusion

[30] The main objective of this work was to perform an experimental validation of the numerical model which was developed to determine the equilibrium electric potential of the Rosetta orbiter in the inner coma of comet Wirtanen. Space plasma simulation chambers, such as the JONAS facility where the experiment was conducted, are designed

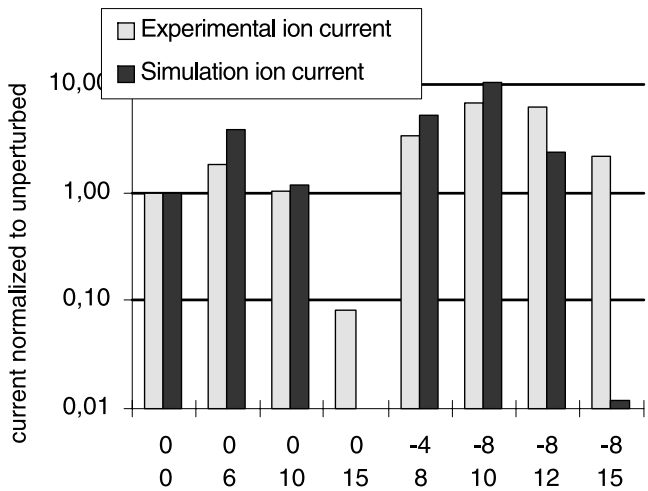

Figure 10. Same as Figure 9, but for hole diameter in the face of the mock-up: 40 mm.

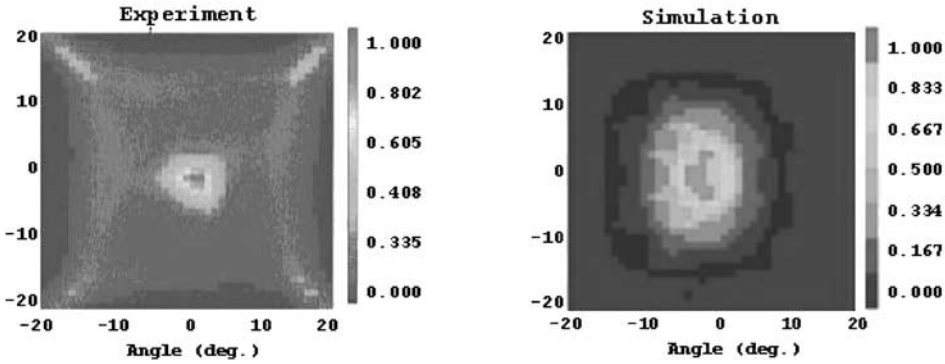

Figure 11. Comparison between ion angular distribution function from the numerical simulation and the experiment. See color version of this figure at back of this issue.

to simulate the plasma conditions encountered on LEO orbits and cannot produce plasmas with cometary characteristics, especially the very low ion and electron temperatures. In order to perform a meaningful validation of the numerical model, we were therefore lead to use similarity laws to define scaled plasma characteristics that simulate the cometary conditions. The laboratory conditions that have been achieved in practice during the tests were constrained by the practical limitations imposed by the operation of the plasma source but we have been able to find a set of conditions that are good representative of the physics of the problem. This is identical to what is done in aerodynamic wind tunnel experiments. The photoelectron emission was not simulated because the energy of the photoelectrons cannot be scaled. This is not a strong limitation since the essential effect of photoelectron emission, as shown by numerical simulations, is to drive positive the spacecraft potential. Indeed, in the nominal position 1 of the spacecraft, the photoelectron trajectories do not bend back to the side of the spacecraft opposite to the Sun and which faces the nucleus and have thus no effect on the structure of this region of the sheath which is of interest for us. During the tests, the various faces of the spacecraft and solar panels mock-up were electrically insulated in order to simulate the ''insulator'' electrical configuration studied in the numerical simulation. Various potential configurations have thus allowed to simulate the electrical equilibrium of the orbiter and solar panels which may vary significantly from one configuration to the other.

[31] The tests were conducted with a 1/10 scaled model of the orbiter equipped on each side with plates simulating the solar panels. In the middle of the face looking towards the plasma source, i.e., the comet nucleus, a hole allowed ions to impinge on the polarisable entrance plate of an ion analyzer internal to the mock-up and eventually to be detected. The approach of our work was to run the numerical model with boundary conditions exactly identical to those in the chamber and compare the results with experimental measurements.

[32] We first considered the global scale by looking at the total currents collected on the various faces of the mock-up of the orbiter and solar panels. There is a very good agreement between the model and the experiment for the whole set of potentials which were imposed, both positive and negative, uniform and non uniform on the external surfaces of the mock-up. This demonstrates the capability of the model to take correctly into account the dynamics of both ions and electrons and gives confidence in the floating potential calculations. Furthermore we may point out that when the mock-up was polarized positively, the typical energy of the electrons in the sheath was several volts. This energy is similar to the energy of the photoelectrons which, in the cometary case, control the sheath on the sunward half space of the spacecraft and are a dominant term of the charging process. The validation of the model for the determination of a sheath structure with electrons of a similar energy gives confidence in its ability to describe correctly the sunward sheath in the cometary case and therefore the amplitude of the charging.

[33] We then considered a smaller scale by comparing ion currents collected on the entrance plate of the analyzer. Again the agreement is good for the various configurations of polarization of the orbiter mock-up and entrance of the analyzer. A systematic deficiency of the experimental currents with respect to the modeled ones can be explained by the simplification of the geometrical description of the entrance area of the analyzer imposed by the finite mesh size of the numerical grid.

[34] The last comparison was made on a very detailed scale by looking at the angular distribution of ions detected by the analyzer. The measured angular distribution is narrower than the numerical one. Two reasons can explain the discrepancy: the difference between the actual geometry of the analyzer entrance and the simplified one used in the simulation and the limited resolution of the computational grid in the model.

[35] In conclusion the experimental tests gave global results which are in very good agreement with model expectations and provide confidence in the capability of the model to correctly describe the sheath structure and current collection and to predict the electrical equilibrium of the Rosetta spacecraft. Such a laboratory validation can very seldom be performed in the field of numerical simulation and we believe it is of very high interest not only for the study that we have undertaken but also to demonstrate the general validity of the model. We intend in the future to improve the resolution of the numerical model in order to study more accurately the ion collection by instruments on Rosetta and, possibly, to make more detailed experimental tests with an improved version of the mock-up.

[36] **Acknowledgments.** We wish to thank Eamon Daly and Alain Hilgers from ESTEC/TOS-EMA for their continuous support and useful discussions in the course of the study. This study was undertaken under the auspices of the ESA contract 12398/97/NL/MV. We acknowledge the referee for his comments that helped to improve the presentation of the paper.

[37] Shadia Rifai Habbal thanks David N. Walker and another referee for their assistance in evaluating this paper.

References

Baker, K. D., N. Singh, L. P. Block, R. Kist, W. Kampa, and H. Thiemann (1981), Studies of strong laboratory double layers and comparison with computer simulation, *J. Plasma Phys.*, *26*, 1–27.

Bernstein, W., J. O. McGarity, and A. Konradi (1983), Electron beam infection experiments: Replication of flight observations in a laboratory beam plasma discharge, *Geophys. Res. Lett.*, *10*, 1124–1127.

Bourham, M., et al. (2002), Electrostatic interaction between Interball-2 and the ambient plasma. 1- Determination of the spacecraft potential from current calculations, *Ann. Geophys.*, *20*, 365–376.

Coggiola, E. (1998), Etude théorique et expérimentale de l'écoulement de plasma autour d'un cylindre non equipotentiel, Thèse de Doctorat, Ecole Nationale Supérieure de l'Aéronautique et de l'Espace, Toulouse, France.

Erukhimov, L. M., and L. G. Genkin (1992), The ionosphere as a space plasma laboratory (in Russian), *Izv. Vyssh. Uchebn. Zaved. Radiofiz.*, *35*, 863–888.

Grün, E., H. Kochan, and K. J. Seidensticker (1991), Laboratory simulation, a tool for comet research, *Geophys. Res. Lett.*, *18*, 245–248.

Hamelin, M., M. Bouhram, N. Dubouloz, M. Malingre, S. A. Grigoriev, and L. V. Zinin (2002), Electrostatic interaction between Interball-2 and the ambient plasma 2, Influence on the low energy ion measurements with Hyperboloïd, *Ann. Geophys.*, *20*, 377–390.

Hesselbarth, P., D. Krankowsky, P. Lämmerzhal, K. Mauesberger, A. Winkler, P. Hsiung, and K. Rössler (1991), Gas release from ice/dust mixtures, *Geophys. Res. Lett.*, *18*, 269–272.

Kellog, P. J., et al. (1982), Laboratory simulation of injection of particle beams in the ionosphere, in *Artificial Particle Beams in Space Plasma Physics*, edited by B. Grandal, pp. 289–329, Plenum, New York.

Kömle, N. I., G. Steiner, M. Baguhl, H. Kohl, H. Kochan, and K. Thiel (1991), The effect of non-volatile porous layers on temperature and vapor pressure of underlying ice, *Geophys. Res. Lett.*, *18*, 265–268.

Koons, H. C., M. H. Dazey, and B. C. Edgar (1984), Impedance measurements on a VLF multiturn antenna in a space plasma simulation chamber, *Radio Sci.*, *19*, 395–399.

Mendis, D. A., H. L. F. Houpis, and M. L. Marconi (1985), The physics of comets, *Fund. Cosmic Phys.*, *10*, 1–380.

Podgornyi, I. M., and R. Z. Sagdeev (1970), Physics of interplanetary plasma and laboratory experiments, *Soviet Phys. Usp.*, *12*, 445.

Roussel, J.-F., and J.-J. Berthelier (2003), A study of the electrical charging of the Rosetta orbiter: 1. Numerical model, *J. Geophys. Res.*, *109*, doi:10.1029/2003JA009836, in press.

Roussel, J.-F., V. Viel, and J. Bernard (1997), Characterization of a multicomponent plasma in an ionospheric plasma simulation chamber, paper presented at International Conference on Phenomena in Ionized Gases, Univ. Paul Sabatier, Toulouse, France.

Svenes, K. R., and J. Troim (1994), Laboratory simulation of vehicle-plasma interaction in low Earth orbit, *Planet. Space Sci.*, *42*, 81–94.

Tsutui, M., H. Matsumoto, and I. Kimura (1984), Laboratory simulation of low-energy electron beam injection by a Japanese sounding rocket in space, *Radio Sci.*, *19*, 503–508.

Vannaroni, G., R. Giovi, and F. de Venuto (1992), Laboratory simulation of the interaction between a tethered satellite system and the ionosphere, *Il Nuovo Cimento*, *15*, 685–701.

Wright, K. H., Jr., N. H. Stone, and U. Samir (1985), A study of plasma expansion phenomena in laboratory generated plasma wakes: Preliminary results, *J. Plasma Phys.*, *33*, 71–82.

J.-J. Berthelier, Centre d'étude des Environnements Terrestre et Planétaires (CETP), 4 Av. de Neptune, 94100 St Maur des Fossés, France. (jean-jacques.berthelier@cetp.ipsl.fr)

J.-F. Roussel, Office National d'Etudes et de Recherches Aérospatiales (ONERA), Département Environnement Spatial (DESP), 2 Av. Edouard Belin, 31055 Toulouse Cedex, France. (roussel@onecert.fr)

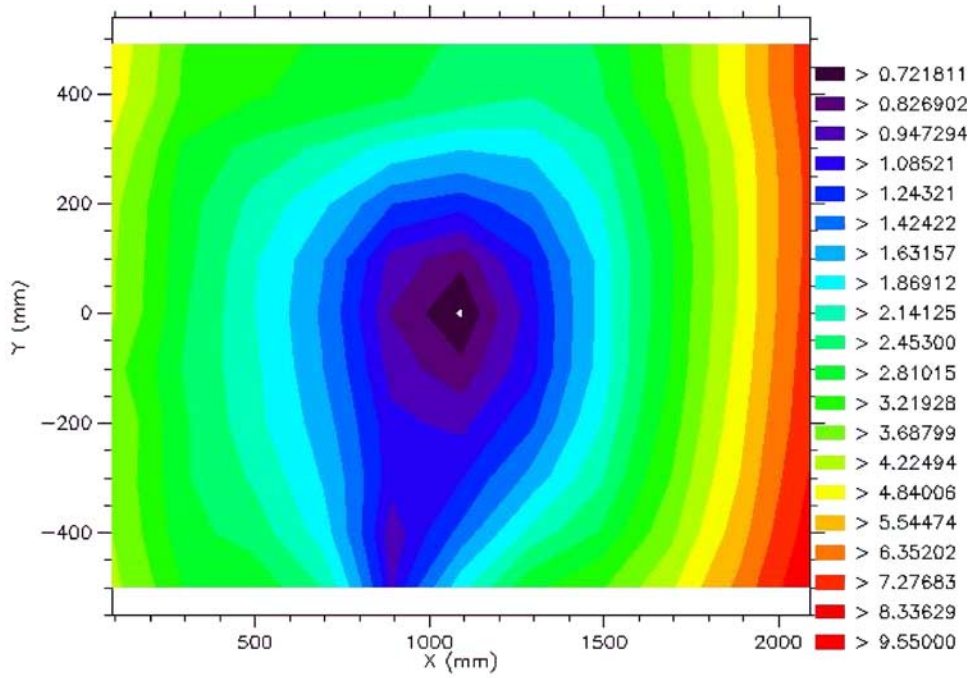

Figure 1. Norm of the compensated magnetic field in the symmetry plane of JONAS chamber (μT).

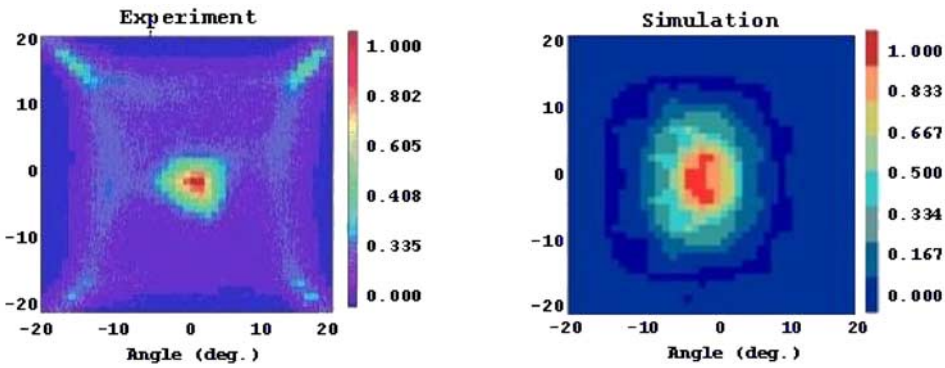

Figure 11. Comparison between ion angular distribution function from the numerical simulation and the experiment.